Article

Synthesis and Characterization of *meso*-Triarylsubporphyrins

Yuichi Takeuchi, Atsushi Matsuda, and Nagao Kobayashi

J. Am. Chem. Soc., **2007**, 129 (26), 8271-8281• DOI: 10.1021/ja0712120 • Publication Date (Web): 08 June 2007

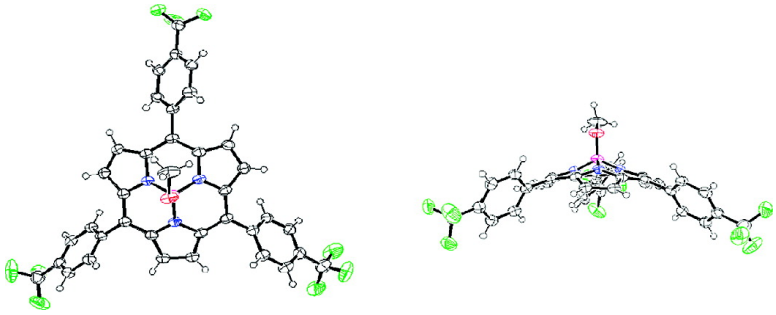

J|A|C|S
ARTICLES
Published on Web 06/08/2007

Synthesis and Characterization of *meso*-Triarylsubporphyrins

Yuichi Takeuchi, Atsushi Matsuda, and Nagao Kobayashi*

Contribution from the Department of Chemistry, Graduate School of Science, Tohoku University, Sendai 980-8578, Japan

Received March 5, 2007; E-mail: nagaok@mail.tains.tohoku.ac.jp

Abstract: The synthesis of several *meso*-triaryl-subporphyrins, based on utilizing tripyrrolylborane as a precursor in a reaction with arylaldehydes (where aryl = phenyl, 4- and 3-pyridyl, tolyl, 4-methoxyphenyl, and 4-(trifluoromethyl)phenyl) under reflux in propionic acid, is reported. All of the compounds have been successfully characterized by ^{1}H−, ^{13}C−, and ^{13}C−^{1}H 2D NMR, electronic absorption, magnetic circular dichroism (MCD), IR, and fluorescence spectroscopy, together with cyclic (CV) and differential pulse (DPV) voltammetry. The X-ray structure of tris{(trifluoromethyl)phenyl}subporphyrin was found to be slightly domed and similar to that of the recently reported hexaethylsubtriazaporphyrin (*Inorg. Chem.* **2006**, *45*, 6148). The electronic absorption spectra of all of the subporphyrins contain intense Soret bands in the 370−380 nm region and weaker Q bands in the 420−550 nm region, which are at shorter wavelengths than those observed (at *ca.* 400−420 nm and *ca.* 450−650 nm, respectively) for tetrapyrrole porphyrins. The intensity of the Q_{00} band decreases as the *meso*-aryl groups become more electron withdrawing. These characteristics can be rationalized by using Gouterman's four-orbital model as a conceptual framework. The MCD bands observed in the Q band region of the subporphyrins (subPs) spectra consistently show a −ve/+ve intensity pattern in ascending energy, while, in contrast, the sign sequence of the bands observed in the Soret band region change dramatically depending on the nature of the aryl groups: from +ve/−ve in the case of the electron withdrawing 4-pyridyl, 4-(trifluoromethyl)phenyl and 3-pyridyl groups to −ve only for phenyl and −ve/+ve for the electron donating 4-tolyl and 4-methoxyphenyl groups. S1 fluorescence emission was observed in the 490−620 nm region. The quantum yields (ϕ_F) in benzene (ϕ_F = 0.10−0.12) are similar to that of metal-free tetraphenylporphyrin (H_2TPP) (ϕ_F = 0.11) but are somewhat lower in the case of ethanol (ϕ_F = 0.06−0.07) due to the higher polarity. The redox potential differences observed between the first oxidation and reduction steps are in the 2.52−2.64 V range, which is larger than that of normal porphyrins (ca. 2.25 V). Molecular orbital (MO) calculations of these compounds help to provide an enhanced understanding of the spectroscopic and electrochemical properties. A byproduct of the synthesis was characterized using X-ray crystallography and a range of spectroscopic techniques. A subporphyrin μ-oxo dimer was prepared and characterized.

Introduction

Porphyrins normally consist of four pyrrole rings linked by *meso*-carbons at the α-pyrrole carbons. Tetraphenylporphyrins (TPPs) and octaethylporphyrins (OEPs) have been examined most intensively due to their easy synthesis, in the case of TPPs, and relevance to biologically important porphyrins, in the case of OEPs. Many types of porphyrin analogues have been reported, which deviate from the basic tetrapyrrole structure.[1] Ring-expanded porphyrins have been known for many years. The so-called pentaphyrins, consisting of five pyrrole rings, Figure 1, are one of the most significant.[2] In the case of azaporphyrins, in which the *meso*-carbons are replaced by aza-nitrogens, the tetrabenzotetraazaporphyrins (or phthalocyanines (Pcs)) have been used for a variety of practical applications over the past 70 years,[3,4] while research on tetraazaporphyrins only became significant in the mid-1970s.[5] Very few ring-expanded azaporphyrins have been reported. The first example of a superphthalocyanine (SPc) consisting of five isoindoledi-

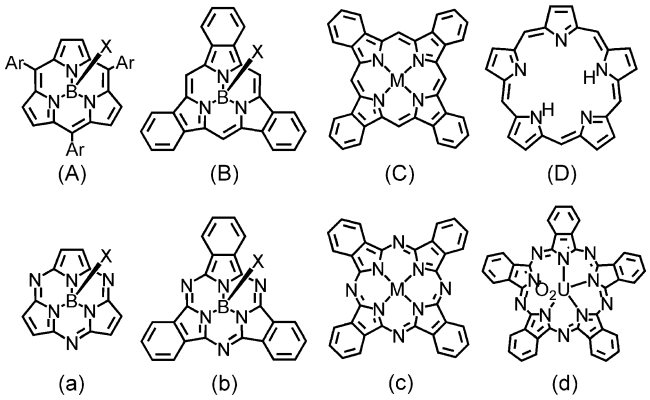

Figure 1. Structures of (A) triarylsubporphyrin (subP), (B) tribenzosubporphyrin, (C) tetrabenzoporphyrin (TBP), (D) pentaphyrin, (a) triazasubporphyrin (subAP), (b) subphthalocyanine (subPc), (c) phthalocyanine (Pc), and (d) superphthalocyanine (SPc).

(1) *The Porphyrin Handbook*; Kadish, K. M., Smith, K. M., Guilard, R., Eds.; Academic Press: San Diego, 2000; Vol. 2.
(2) Sessler J. L.; Gebauer, A.; Weghohn, S. J. In *The Porphyrin Handbook*; Kadish, K. M., Smith, K. M., Guilard, R., Eds.; Academic Press: San Diego, 2000; Vol. 2, Chapter 9.

imine units was synthesized in 1964 and characterized by X-ray crsytallography in 1975.[6] The first ring-contracted azaporphyrin congener, consisting of three isoindolediimine units, subphthalocyanine (subPc), was prepared in 1972,[7] and its structure was confirmed by X-ray crystallography in 1974.[8] The importance of subPcs in the field of phthalocyanine synthesis was recognized in 1990 when it was found that they undergo a ring-expansion reaction with isoindolediimine derivatives that results in the preferential formation of a monosubstituted type of reduced symmetry metal-free Pcs.[9] Since then, more than a hundred papers have appeared on subPc and its derivatives.[10,11] In contrast, the first report of a subporphyrin (subP) was made by Osuka's group as recently as 2006,[12] when the synthesis of tribenzosubporphyrins was reported. The structure was found to be domed in a similar manner to the subPcs. Tribenzosubporphyrin can be regarded as a ring-contracted tetrabenzoporphyrin. Since the electronic properties of tetrabenzoporphyrins differ significantly from those of porphyrins due to the presence of fused benzene rings, the synthesis of subporphyrins without fused benzene rings is still clearly required to enable a direct comparison of the properties of subporphyrins to those of tetrapyrrole porphyrins. In this paper, we report the synthesis and properties of *meso*-triarylsubporphyrins and use DFT and TD-DFT calculations to rationalize many of the observed experimental properties and trends.

Experimental Section

Measurements. Electronic absorption spectra were recorded with Hitachi U-3410 and JASCO V-570 spectrophotometers. Magnetic circular dichroism (MCD) spectra were recorded with a JASCO J-725 spectrodichrometer equipped with a JASCO electromagnet, which produces magnetic fields of up to 1.09 T (1 T = 1 tesla) with both parallel and antiparallel fields. The magnitudes were expressed in terms of molar ellipticity per tesla ($[\theta]_M$/deg dm^3 mol^{-1} cm^{-1} T^{-1}). Fluorescence spectral measurements were made with a Hitachi F-4500 spectrofluorimeter with appropriate filters installed to eliminate scattered light. Fluorescence quantum yields (ϕ_F) were determined by using 9,10-diphenylanthracene in benzene ($\phi_F = 0.84$) or ethanol ($\phi_F = 0.81$)[13] as the standard. Data were obtained by the comparative calibration method, by using the same excitation wavelength and absorbance for the subP samples and the calibrant, as well as the same emission energies. All solutions for fluorescence measurements were purged with argon prior to measurement, and the absorbance of the solution at the excitation wavelength (366 nm in benzene and ethanol) was always less than 0.1. FTIR and ^{1}H NMR spectra were recorded with Shimadzu FTIR-8100M and FTIR 8600PC spectrometers using KBr disks and with a JEOL GSX-400 spectrometer using $CDCl_3$, respectively. The ^{13}C and ^{13}C−^{1}H two-dimensional NMR measurements were made using a JEOL ECA-600 spectrometer with $CDCl_3$ as the solvent. Size exclusion chromatography was conducted using a JAI LC9201 HPLC instrument with Jaigel 3H, 2.5H, and 2H columns with $CHCl_3$ as the eluent. Mass spectra were recorded on Perspective Biosystem MALDI-TOF Mass Voyager DCE-S12 and Micromass LCT ESI-TOF MS spectrometers using methanol as a solvent. HRMS was recorded on a Bruker Daltonics Apex-III spectrometer using $CHCl_3$/MeOH as the solvent.

X-ray crystallographic studies were carried out on a Rigaku Saturn CCD spectrometer with graphite monochromatized Mo Kα radiation ($\lambda = 0.710\ 73$ Å). Data were collected at 150 and 173 K, respectively, for tris{4-(trifluoromethyl)phenyl}subporphyrin and a boron−dipyrromethene complex, which was isolated as a major byproduct during the synthesis of the former. The structures were derived using the SHELXS-97 program and refined on F^2 using the SHELXL-97 program.[14]

CV and DPV measurements were recorded with a Hokuto Denko HZ5000 potentiostat under purified nitrogen in *o*-dichlorobenzene (DCB) (Nakalai Tesque) solutions with tetrabutylammonium perchlorate (TBAP, 0.1 mol/L) as the supporting electrolyte. Measurements were made with a glassy carbon electrode (area = 0.07 cm^2), a Ag/AgCl reference electrode, and a Pt wire counter electrode. The concentration of the solution was fixed at 0.5 mmol/L, and the sweep rates were 100 mV/s and 10mV/s for CV and DPV measurements, respectively. The ferrocene/ferrocenium (Fc/Fc^+) couple was used as the internal standard.

Molecular Orbital Calculations. The Gaussian 03 software package[15] was used to carry out DFT and TD-DFT calculations using the B3LYP functional with 6-31G(d) basis sets.[16] An optimum scaling factor of 0.9614 was applied[17] to calculated IR frequencies to enable comparison with the experimentally obtained data of PhsubP (**2a**).

Synthesis. Tripyrrolylborane (1).[18] Lithium borohydride (250 mg, 11.5 mmol) was dissolved in 4.5 mL (65.1 mmol) of freshly distilled pyrrole and was refluxed under nitrogen in the dark until evolution of hydrogen had ceased (*ca.* 6−8 h). Unreacted pyrrole was removed from the emulsion *in vacuo*, and the residue was dissolved in dry diethyl ether. Boron trifluoride ethyl ether complex (2.0 mL, 15.9 mmol) was added dropwise under stirring for 10 min, and the solution was then refluxed for a further 15 min and then cooled. The resulting residue was collected by filtration, washed three times with the filtrate, and recrystallyzed from toluene, to give 1.5 g (7.4 mmol) of the target compound as a white powder in 64% yield. ^{1}H NMR ($CDCl_3$): δ = 6.26 (s, 6H, pyrrole-β), 6.82 (s, 6H, pyrrole-α) ppm. Since this compound is photolabile, it should be used immediately for the next reaction step. If the reaction is carried out without shielding from light, the yield is reduced to *ca.* 25%.

***meso*-Triphenylsubporphyrin (2a) (PhsubP).** Tripyrrolylborane (0.1 g, 0.48 mmol) was dispersed in propionic acid (35 mL). The solution was added slowly dropwise to a refluxing solution of benzaldehyde (*ca.* 0.1 mol/L, 3.5 mmol)[19] in propionic acid (35 mL) over

(3) *Phthalocyanines-Properties and Applications*; Leznoff, C. C., Lever, A. B. P., Eds.; VCH: Weinheim, 1989, 1992, 1993, 1996.
(4) *Phthalocyanines-Chemistry and Functions*; Shirai, H., Kobayashi, N., Eds.; IPC: Tokyo, 1997.
(5) Kobayashi, N. In ref 1, Chapter 13.
(6) (a) Bloor, J. E.; Schlabitz, J.; Wallden, C. C.; Demerdache, A. *Can. J. Chem.* **1964**, *42*, 2201. (b) Day, V. W.; Mark, T. J.; Wacher, W. A. *J. Am. Chem. Soc.* **1975**, *97*, 4519.
(7) Meller, A.; Ossko, A. *Monatsh. Chem.* **1972**, *103*, 150.
(8) Kietaibl, H. *Monatsh. Chem.* **1974**, *105*, 405.
(9) Kobayashi, N.; Kondo, R.; Nakajima, S.; Osa, T. *J. Am. Chem. Soc.* **1990**, *112*, 9640−9641.
(10) (a) Kobayashi, N. In *The Porphyrin Handbook*; Kadish, K. M., Smith, K. M., Guilard, R., Eds.; Academic Press: San Diego, 2004; Vol. 15, Chapter 100, pp 161−262. (b) Kobayashi, N. *Chem. Commun.* **1991**, 1203. (c) Kobayashi, N.; Ishizaki, T.; Ishii, K.; Konami, H. *J. Am. Chem. Soc.* **1999**, *121*, 9096. (d) Fukuda, T.; Stork, J. R.; Potucek, R. J.; Olmstead, M. M.; Noll, B. C.; Kobayashi, N.; Durfee, W. S. *Angew. Chem., Int. Ed.* **2002**, *41*, 2565. (e) Fukuda, T.; Olmstead, M. M.; Durfee, W. S.; Kobayashi, N. *Chem. Commun.* **2003**, 1256.
(11) (a) Torres, T. *Angew. Chem., Int. Ed.* **2006**, *45*, 2834. (b) Claessens, C. G.; Torres, T. *Chem. Rev.* **2002**, *102*, 835. (c) Sastre, A.; Torres, T.; Diaz-Garcia, M. A.; Agullo-Lopez, F.; Dhenaut, C.; Brasselet, S.; Ledoux, I.; Zyss, J. *J. Am. Chem. Soc.* **1996**, *118*, 2746. (d) Diaz-Garcia, M. A.; Agullo-Lopez, F.; Sastre, A.; Torres, T.; Torruellas, W. F.; Stegeman, G. I. *J. Phys. Chem.* **1995**, *99*, 14988.
(12) Inokuma, Y.; Kwan, J. H.; Ahn, T. K.; Yoon, M. C.; Kim, D.; Osuka, A. *Angew. Chem., Int. Ed.* **2006**, *45*, 961.
(13) Birks, J. B.; Dyson, D. J. *Proc. R. Soc. London, Ser. A* **1963**, *275*, 135.
(14) Sheldrick, G. M. *SHELXS 97 and SHELXL 97, Program for the Solution and Refinement of Crystal Structures*; University of Goettingen: Goettingen, Germany, 1997.
(15) Frisch, M. J., et al. *Gaussian 03*, revision C.02; Gaussian Inc.: Wallingford, CT, 2004.
(16) (a) Stratmann, R. E.; Scuseria, G. E.; Frisch, M. J. *J. Chem. Phys.* **1988**, *109*, 8218. (b) Bauernschmitt, R.; Ahlrichs, R. *Chem. Phys. Lett.* **1996**, *256*, 454. (c) Casida, M. E.; Jamorski, C.; Casida, K. C.; Salahub, D. R. *J. Chem. Phys.* **1988**, *108*, 4439.
(17) (a) Scott, A. P.; Radom, L. R. *J. Phys. Chem.* **1996**, *100*, 16502. (b) Wong, M. W. *Chem. Phys. Lett.* **1996**, *256*, 391.
(18) Gyori, B.; Emri, J.; Szarvas, P. *Acta Chim. (Budapest)* **1975**, *86*, 235.
(19) Almog, J.; Baldwin, J. E.; Crossley, M. J.; Debernardis, J. F.; Dyer, R. L.; Huff, M. K. *Tetrahedron* **1981**, *37*, 3589.

45 min. The progress of the reaction was monitored by periodically measuring the absorption spectra of the reaction solution. The solution was then heated under reflux for a further 3−4 h until the absorbance of a PhsubP (**2a**) peak at 373 nm ceased to increase. The solvent was removed. The residue was dissolved in $CHCl_3$ and then passed through a short column of Celite to remove undissolved materials. Subsequently, purification was performed using silica gel chromatography ($CHCl_3$/MeOH = 100:1, 75:1, 25:1 v/v) and silica gel TLC (toluene/MeOH = 25:1 v/v), which was repeated three times. PhsubP (**2a**) was obtained as an orange-yellow powder in *ca.* 6% yield. ^{1}H NMR ($CDCl_3$): δ 7.60 (t, J = 7.6 Hz, 3H, aryl-*p*), 7.69 (dd, J_1 = 7.9 Hz, J_2 = 7.6 Hz, 6H, aryl-*m*), 8.06 (d, J = 7.9 Hz, 6H, aryl-*o*), 8.12 (s, 6H, pyrrole-β) ppm. ^{13}C NMR ($CDCl_3$) δ 120.3 (*meso*), 122.3 (pyrrole β), 127.8 (aryl-*p*), 128.7 (aryl-*m*), 133.2 (aryl-*o*), 137.2 (C_{ipso} of phenyl), 140.4 (pyrrole α) ppm. IR (KBr) 3445, 2919, 2849, 1733, 1505, 1458, 1265, 1153, 792, 727, 700, 419 cm^{-1}. HR-ESI-MS *m*/*z* 470.1820 [M−OH]$^+$; calcd for $C_{33}N_3H_{21}B$ [M−OH]$^+$ 470.1829. UV/vis ($CDCl_3$) $\lambda_{max}(\epsilon)$ 486 (8000), 461 (12 000), 373 (151 000) nm.

***meso*-Tritolylsubporphyrin (2b) (TLsubP).** A similar procedure to that above was used with *p*-tolualdehyde replacing benzaldehyde. TLsubP (**2b**) was obtained as an orange powder in *ca.* 7% yield. A $CHCl_3$/MeOH solvent mixture was used in 50:1, 50:1, 40:1 v/v ratios during silica gel chromatography, while a 25:1 v/v ratio of toluene/MeOH was used twice during TLC. ^{1}H NMR ($CDCl_3$): δ 2.57 (s, 9H, CH_3), 7.50 (d, J = 7.9 Hz, 6H, aryl-*m*), 7.95 (d, J = 7.9 Hz, 6H, aryl-*o*), 8.10 (s, 6H, pyrrole-β) ppm. ^{13}C NMR ($CDCl_3$) δ 21.3 (*Me*), 120.23 (*meso*), 122.3 (pyrrole β), 129.4 (aryl-*m*), 133.0 (aryl-*o*), 134.3 (C_{ipso} of phenyl), 137.5 (aryl-*p*), 140.2 (pyrrole α) ppm. IR (KBr) 3445, 2921, 2851, 1716, 1515, 1457, 1340, 1267, 1153, 1018, 827, 792, 729 cm^{-1}. HR-ESI-MS *m*/*z* 512.2289 [M−OH]$^+$; calcd for $C_{36}N_3H_{27}B$ [M−OH]$^+$ 512.2298. UV/vis ($CDCl_3$) $\lambda_{max}(\epsilon)$ 490 (10 000), 463 (11 000), 376 (148 000) nm.

***meso*-Tri(4-pyridyl)subporphyrin (2c) (4PysubP).** The procedure used for the synthesis of PhsubP (**2a**) was repeated using 4-pyridinecarboxyaldehyde instead of benzaldehyde, and a reddish orange powder was obtained in *ca.* 4% yield. A $CHCl_3$/MeOH solvent mixture was used in a 25:1 v/v ratio during silica gel chromatography, while a 25:1 v/v ratio of toluene/MeOH was used twice during TLC. The product was then purified by HPLC using $CHCl_3$. ^{1}H NMR ($CDCl_3$): δ 7.99 (d, J = 5.7 Hz, 6H, pyridyl-*o*), 8.19 (s, 6H, pyrrole-β), 8.97 (d, J = 5.7 Hz, 6H, pyridyl-*m*) ppm. ^{13}C NMR ($CDCl_3$) δ 118.1 (*meso*), 122.8 (pyrrole β), 127.7 (pyridyl-*o*), 140.5 (pyrrole α), 144.7 (C_{ipso} of pyridyl), 150.0 (pyridyl-*m*) ppm. IR (KBr) 3445, 2924, 2855, 1716, 1594, 1458, 1271, 1159, 1072, 833, 796, 729, 681, 419 cm^{-1}. HR-ESI-MS *m*/*z* 491.1786 [M]$^+$; calcd for $C_{30}N_6H_{20}BOH$ [M]$^+$ 491.1792. UV/vis ($CDCl_3$) $\lambda_{max}(\epsilon)$ 460 (13 000), 373 (148 000) nm.

***meso*-Tri(3-pyridyl)subporphyrin (2d) (3PysubP).** The synthesis was carried out in the same manner as that for 4PysubP (**2c**) by using 3-pyridinecarboxyaldehyde instead of 4-pyridinecarboxyaldehyde. 3PysubP (**2d**) was obtained as an orange powder in 6% yield. ^{1}H NMR ($CDCl_3$): δ 7.67 (dd, J_1 = 7.9 Hz, J_2 = 4.8 Hz, 3H, pyridyl-*m*), 8.13 (s, 6H, pyrrole-β), 8.39 (d, J = 7.9 Hz, 3H, pyridyl-*o*), 8.87 (d, J = 4.8 Hz, 3H, pyridyl-*p*), 9.24 (s, 3H, pyridyl-*o*′) ppm. HR-ESI-MS *m*/*z* 473.1680 [M−OH]$^+$; calcd for $C_{30}N_6H_{20}B$ [M−OH]$^+$ 473.1686. UV/vis ($CDCl_3$) $\lambda_{max}(\epsilon)$ 480sh (6400), 458 (12 000), 371 (149 000) nm.

***meso*-Tri(4-methoxyphenyl)subporphyrin (2e) (MOsubP).** The synthesis of MOsubP (**2e**) was carried out in a similar manner to that of 4PysubP (**2c**) by using anisaldehyde instead of 4-pyridinecarboxyaldehyde. The solvents used were $CHCl_3$/MeOH in 30:1 and 75:1 v/v ratios during the silica gel chromatography step, $CHCl_3$ for alumina chromatography, toluene/MeOH in a 25:1 v/v ratio three times during TLC, and $CHCl_3$ for HPLC. The yield was *ca.* 8%. ^{1}H NMR ($CDCl_3$): δ 3.97 (s, 9H, OCH_3), 7.22 (d, J = 8.7 Hz, 6H, aryl-*m*), 7.99 (d, J = 8.7 Hz, 6H, aryl-*o*), 8.08 (s, 6H, pyrrole-β) ppm. ^{13}C NMR ($CDCl_3$) δ 55.5 (*Me*O), 114.2 (aryl-*m*), 119.9 (*meso*), 122.0 (pyrrole β), 129.7 (C_{ipso} of phenyl), 134.1 (aryl-*o*), 140.4 (pyrrole α), 159.6 (aryl-*p*) ppm. IR (KBr) 2928, 2830, 1604, 1515, 1458, 1340, 1286, 1247, 1174, 1028, 835, 791, 731, 613 cm^{-1}. HR-ESI-MS *m*/*z* 560.2138 [M−OH]$^+$; calcd for $C_{36}N_3H_{27}BO_3$ [M−OH]$^+$ 560.2145. UV/vis ($CDCl_3$) $\lambda_{max}(\epsilon)$ 496 (14 000), 466 (11 000), 379 (154 000) nm.

Scheme 1. Synthetic Pathway to Triarylsubporphyrins

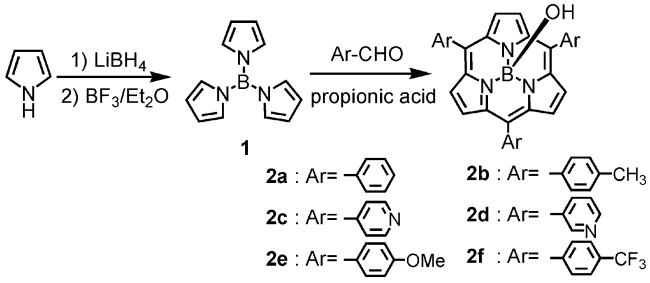

***meso*-Tris{(4-trifluoromethyl)phenyl}subporphyrin (2f) (TFsubP).** The synthesis of TFsubP (**2f**) was carried out in a similar manner to that of 4PysubP (**2c**) by using (4-trifluoromethyl)benzaldehyde instead of 4-pyridinecarboxyaldehyde. $CHCl_3$/MeOH in 100:1 and 1:0 v/v ratios was used for the silica gel chromatography step, while toluene/MeOH = 25:1 v/v was used for the subsequent TLC. The residue was further purified by HPLC using $CHCl_3$ as the eluent, and TFsubP (**2f**) was finally crystallized from CH_2Cl_2 and MeOH, to give reddish orange needles in *ca.* 4% yield. ^{1}H NMR ($CDCl_3$): δ 7.98 (d, J = 7.9 Hz, 6H, aryl-*o*), 8.13 (s, 6H, pyrrole-β), 8.17 (d, J = 7.9 Hz, 6H, aryl-*m*) ppm. ^{13}C NMR ($CDCl_3$) δ 119.4 (*meso*), 122.6 (pyrrole β), 121.7, 123.5, 125.3, and 127.2 (CF_3), 125.7 (aryl-*m*), 130.3 (aryl-*p*), 133.4 (aryl-*o*), 140.6 (C_{ipso} of phenyl), 141.3 (pyrrole α) ppm. IR (KBr) 2921, 2869, 1716, 1616, 1558, 1540, 1508, 1323, 1166, 1130, 1072, 1018, 983, 850, 792, 725, 604 cm^{-1}. HR-ESI-MS *m*/*z* 674.1440 [M − OH]$^+$; calcd for $C_{36}N_3H_{18}BF_9$ [M − OH]$^+$ 674.1450. UV/vis ($CDCl_3$) $\lambda_{max}(\epsilon)$ 480sh (7000), 460 (13 000), 373 (155 000) nm.

***μ*-Oxo{*meso*-tri(3-pyridyl)subporphyrin} (3) (3PysubP)$_2$O.** *meso*-Tri(3-pyridyl)subporphyrin (3PysubP, **2d**) (5 mg, 7.2×10^{-6} mol) was heated at 80−85 °C *in vacuo* overnight, and the residue was imposed on a HPLC column using $CHCl_3$ as the eluent. The first colored portion was collected (*ca.* 1.9 mg, 38%). ^{1}H NMR ($CDCl_3$): δ 7.58 (m, 6H, pyridyl-*m*), 7.73 (s, 12H, pyrrole-β), 8.10 (d, J = 7.9 Hz, 6H, pyrrole-*o*), 8.83 (d, J = 4.8 Hz, 6H, pyrrole-*p*), 9.03 (s, 6H, pyrrole-*o*′) ppm. MALDI-TOF-MS *m*/*z* 962.92 [M + H]$^+$; calcd for $C_{60}N_{12}H_{36}B_2O$ [M + H]$^+$ 962.33. UV/vis ($CDCl_3$) $\lambda_{max}(\epsilon)$ 465 (7700), 363 (109 000) nm.

Results and Discussion

Synthesis. We successfully synthesized a series of *meso*-triarylsubporphyrins in 4−8% yields by using tripyrrolylborane as the template for an Adler reaction[20] (Scheme 1). Benzaldehyde was first dissolved in propionic acid at 0.1 mol L^{-1}, since this concentration is known to give the highest yield of products in an analogous reaction used to synthesize capped porphyrins.[19] Tripyrrolylborane dispersed in propionic acid was added later, due to a concern that the yield of the desired subPs would be significantly reduced if the N−B bonds were broken. The purification procedure, described in detail in the Experimental Section, was extremely tedious due to the multiple chromatography steps that were required to obtain pure compounds. For example, Figure 2 shows a typical UV−visible absorption spectrum of the reaction solution when the reaction was stopped. Three sharp peaks are observed at 373, 422, and 510 nm. The 422 nm peak is the Soret band of *meso*-tetraphenylporphyrin

(20) Adler, A. D.; Longo, F. R.; Finarelli, J.; Goldmacher, J.; Assour, J.; Korsakoff, L. *J. Org. Chem.* **1967**, *32*, 476.

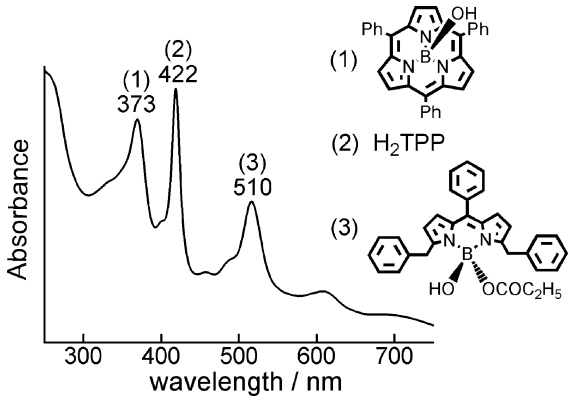

Figure 2. Electronic absorption spectrum recorded at the end of the condensation reaction of PhsubP (**2a**). The solvent consists of a few drops of propionic acid solution diluted by $CHCl_3$. The peaks at 373, 422, and 510 nm are associated with (1) PhsubP (**2a**), (2) H_2TPP, and (3) a boron dipyrromethene derivative, respectively.

(H_2TPP), which is present as a byproduct.[21] The peak at 510 nm is due to another major byproduct and shifts after further purification to 520 nm. In addition to these three compounds, many additional components were detected during TLC experiments. Since the 373 nm band was later found to be the Soret band of subP, and its absorption coefficient was determined to be *ca.* 25% of that of H_2TPP, we were eventually able to estimate that the initial formation yields of subPs were twice those reported in the Experimental Section after purification of each subP, i.e., 8−18%. The yield was higher when arylaldehydes with electron donating character were used.

In order to increase the yield of the desired subPs, the formation of the major byproducts clearly has to be reduced. The 510 nm component in Figure 2 was, therefore, isolated and characterized in order to determine how this might best be accomplished. After tedious chromatography, this component was recrystallized from CH_2Cl_2−MeOH as dark red plate-shaped crystals. X-ray data (see below) confirmed that this red compound was a boron dipyrromethene derivative,[22] i.e. a boron compound containing two pyrrole rings. The absorption and emission spectra are shown in Figure S1. Clearly, one of the three pyrrole rings of the tripyrrolylborane starting material is removed and a B−N bond is partially cleaved. We, therefore, attempted to carry out the subP synthesis by using the milder Lindsey method[23] at room temperature using CH_2Cl_2 containing acid catalysts as the reaction solvent with a subsequent oxidation of the reaction product by DDQ or *p*-chloranil, but this procedure proved unsuccessful even when the reaction temperature was raised to 40 °C.

All six subPs synthesized in this study dissolve readily in a wide range of organic solvents including methanol, ethanol, diethyl ether, hexane, ethyl acetate, acetic acid, chloroform, THF, dioxane, DMF, benzene, toluene, and DMSO, but not in water. The solutions are typically yellow.

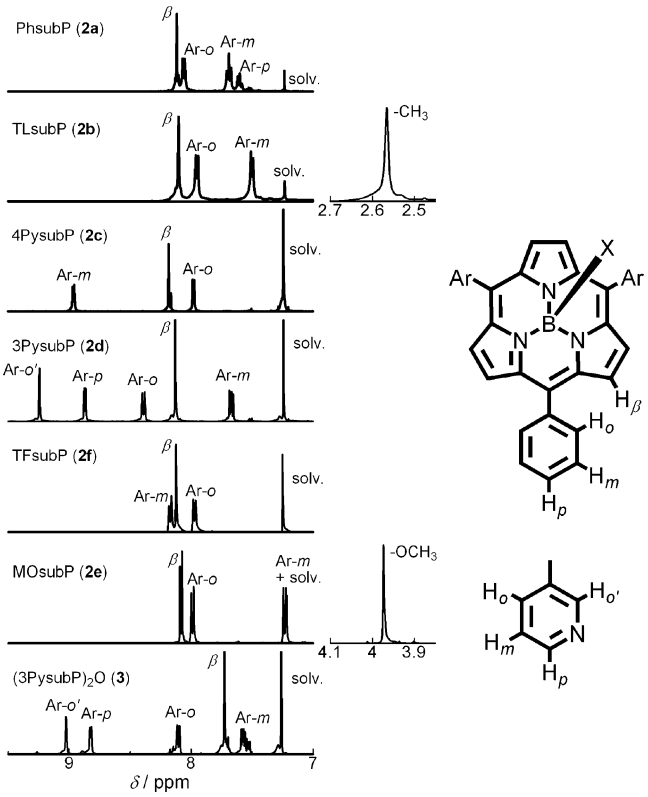

Figure 3. Aromatic region of the ^1H NMR spectra of all six subPs and the μ-oxo dimer (**3**) of 3PysubP (**2d**) recorded in $CDCl_3$. Ar-o′ denotes the *ortho*-proton, which lies next to the pyridyl nitrogen of 3PysubP (**2d**) and $(3PysubP)_2O$ (**3**).

Mass and NMR Spectroscopy. The isotopic distribution patterns observed in the electrospray ionization mass (ESI MS) spectra are in close agreement with those calculated for the boron subP structure, Figure S2. The axial ligands tend to be released upon ionization. Further structural information was derived from ^1H and ^{13}C NMR spectra and $^{13}C-^1H$ 2D experiments. The ^1H NMR spectra of the six subPs and the μ-oxo dimer all exhibit simple spectral patterns reflecting a symmetric C_3 structure, Figure 3. The β-position ^1H peak is observed at 8.1 ppm in the case of PhsubP due to the heteroaromatic nature of the subporphyrin π-system. The downfield shift is not as great as that observed for TPP (8.75 ppm), since the diamagnetic ring current effect is reduced due to the domed structure and the inner ligand perimeter being comprised of a 14 π- rather than an 18 π-electron conjugation system. A similar trend has been observed for analogous macrocycles such as subphthalocyanines,[8] triazasubporphyrin (subAP),[25] and tribenzosubporphyrins.[12] The ^1H NMR signals for the axial ligands are shifted slightly upfield due to diamagnetic ring current effects. A broad peak due to the axial hydroxyl proton is observed at around −2.65 ppm. This hydroxyl group can be replaced with a methoxy group upon refluxing in methanol with the ^1H peak for the axial ligand shifting to 0.83 ppm. The hydroxyl group can be reinserted almost quantitatively by mixing with water.

The ^{13}C NMR spectra exhibit six peaks for 4PysubP (**2c**), seven peaks for PhsubP (**2a**), and eight peaks for TLsubP (**2b**),

(21) *Porphyrins and Metalloporphyrins*; Smith, K. M., Ed.; Elsevier: Amsterdam, 1975; p 876.
(22) λ_{max} (ϵ) 520 (64 800), 343 (11 000) nm in benzene. S1 emission peak = 537 nm, ϕ_F = 0.15 in benzene. Dipyrromethene derivatives of similar structures have been reported recently (McDonnel, S. O.; O'Shea, D. F. *Org. Lett.* **2006**, *8*, 3493. McDonnel, S. O.; Hall, M. J.; Allen, L. T.; Byrne, A.; Gallagher, W. M.; O'Shea, D. F. *J. Am. Chem. Soc.* **2005**, *127*, 16360).
(23) (a) Lindsey, J. S.; Hsu, H. C.; Schreiman, I. C. *Tetrahedron Lett.* **1986**, *27*, 4969. (b) Lindsey, J. S.; Schreiman, I. C.; Hsu, H. C.; Kearney, P. C.; Marguerettaz, A. M. *J. Org. Chem.* **1987**, *52*, 827.
(24) Abraham, R. J.; Hawkes, G. E.; Hudson, M. F.; Smith, K. M. *J. Chem. Soc., Perkin Trans. 2* **1975**, 204.
(25) Stork, J. R.; Brewer, J. J.; Fukuda, T.; Fitzgerald, J. P.; Yee, G. T.; Nazarenko, A. Y.; Kobayashi, N.; Durfee, W. S. *Inorg. Chem.* **2006**, *45*, 6148.

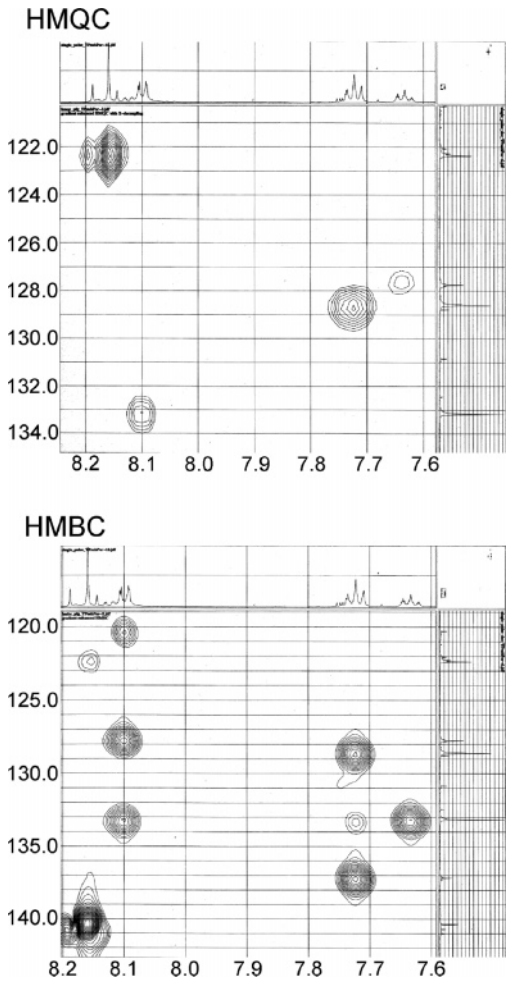

Figure 4. $^{13}C-^{1}H$ HMQC (top) and HMBC (bottom) spectra of PhsubP (**2a**) recorded in $CDCl_3$.

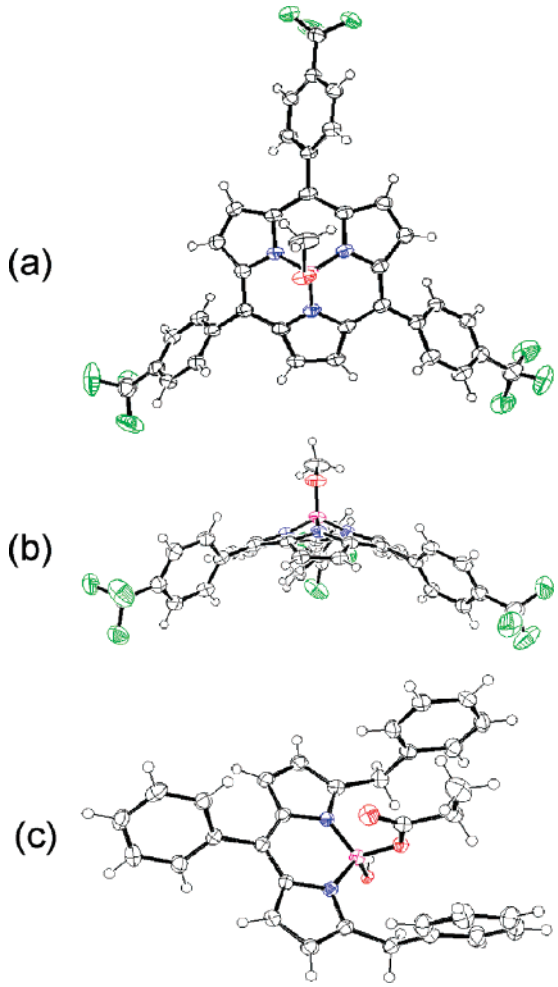

Figure 5. (a) Top and (b) side view of the X-ray structure of TFsubP (**2f**) and (c) side view of the boron dipyrromethene byproduct (see Figure 2, for the molecular structure). The probability level of the thermal ellipsoids is scaled to 50%.

MOsubP (**2e**), and TFsubP (**2f**), respectively, which is consistent with the approximate C_3 symmetry. All the peaks were assigned based on the $^{13}C-^{1}H$ HMQC and HMBC techniques. The spectra of PhsubP (**2a**) are provided as an example, Figure 4 (see Figure S3 for the spectra of TLsubP (**2b**) and MOsubP (**2e**)). Carbon atoms at the α and β pyrrole positions and at the *meso* positions exhibited signals at $\delta = 140-141$, 122−123, and 118−120 ppm, respectively, with only minor spectral differences observed between the compounds. In contrast, the aryl ^{13}C signals shift significantly depending on the nature of the substituents. Signals appear at lower fields when the aryl groups are more electron withdrawing. This trend is also observed for the sp^3 alkyl carbons in the substituents. The carbon atoms of the trifluoromethyl group of TFsubP (**2f**), for example, exhibited signals at low fields of $\delta = 121.7$, 123.5, 125.3, and 127.2 ppm due to coupling between carbon and fluorine atoms. Comparison of the ^{13}C NMR spectra of ZnTPP, H_2TPP,[24] and PhsubP (**2a**) confirms that there is not much difference in the chemical shift observed for the non-phenyl of TPP and subP. Only minor differences are observed in the case of the α and β pyrrole carbons and the *ipso* carbon of phenyl in PhsubP (**2a**). Signals are observed at 5−10, 8−10, and *ca.* 5 ppm higher field, respectively. This, in turn, is probably related to a slight decrease in aromaticity due to the effects of ring-contraction and ligand nonplanarity.

The ^{1}H NMR signals of the μ-oxo dimer of 3PysubP (**2d**), $(3PysubP)_2O$ (**3**), lie at higher fields than those of monomeric 3PysubP (**2d**) due to the additional ring current effect generated by the second subP rings. The splitting pattern was the same as that of 3PysubP (**2d**), which suggests that the two constituent 3PysubP (**2d**) ligands rotate within the NMR time scale.

X-ray Crystallography. Structural confirmation was accomplished by obtaining crystals of TFsubP (**2f**), which were suitable for X-ray analysis by slow diffusion of methanol into a dichloromethane solution. TFsubP (**2f**) exhibits a domed conformation with the boron atom coordinated in tetrahedral fashion by the three pyrrolic nitrogen atoms and an oxygen atom of the methoxy group (Figure 5a, b).[26] The B−N bond distances are 1.505(3), 1.506(3), and 1.514(3) Å. The structure is, therefore, similar to those of subphthalocyanines,[8] subAPs,[25] and tribenzosubporphyrins.[12] The bowl depth as defined by the distance from the boron to the mean plane of the six β-position carbon atoms is 1.430 Å, which is significantly deeper than the 1.175 Å depth observed by Osuka and co-workers[12] for the corresponding methoxy ligated tribenzosubporphyrin.

(26) *meso*-Tris{4-(trifluoromethyl)phenyl}subporphyrin: $C_{37}H_{21}F_9N_3B_1O_1$, $M_W = 705.38$, monoclinic, space group $P2_1/c$ (no. 14), $a = 17.521(5)$ Å, $b = 21.541(6)$ Å, $c = 8.296(2)$ Å, $\beta = 91.057(6)°$, $V = 3130.5(15)$ Å^3, $Z = 4$, $\rho_{calcd} = 1.497$ g/cm^3, $T = -123$ °C. $R = 0.0714$, $R_w = 0.1473$ (all data), GOF = 1.226.

The peripheral bonds of the main TFsubP (**2f**) ligand tend to be longer than those of ZnTPP.[27] For example, the pyrrole(β)−pyrrole(β) and *meso*(C)−pyrrole(α) distances in TFsubP (**2f**) are *ca.* 1.37 and *ca.* 1.42 Å, respectively, while those of ZnTPP[27] are *ca.* 1.35 and *ca.* 1.40 Å. This is probably due to the nonplanarity of the subP π-system. The pyrrole(α)−pyrrole(β) distance (*ca.* 1.44 Å) is approximately the same, however. Although the C(*meso*)−pyrrole(α) bond is longer than the N(*meso*)−pyrrole(α) bond (*ca.* 1.35 Å) in subazaporphyrin, this is clearly due to the presence of a different *meso*-atom. As would be anticipated for an aromatic π-system, almost no bond length alternation is observed in the TFsubP (**2f**) structure.

The angles data also provide strong evidence for a shallow domed tripyrrolic cyclic structure. The average O(axial oxygen)−B−N(pyrrole) angle is 113.8°, which is slightly lower than the 115.6° angle reported for subAP (hexaethyltriazasubporphyrin).[25] In contrast, the N−B−N angle is *ca.* 104.8°, which is higher than the 102.7° value observed in the case of subAP. These data reflect the fact that the depth of the dome is shallower than that of subAP and this, in turn, is related to the smaller central hole size of subAP due to the shorter N(*meso*)−pyrrole-(α) distance. One of the most distinct differences from TPP is that the C(*meso*)−C(pyrrole(α))−C(pyrrole(β)) angle is much larger (133.2°) than that of ZnTPP (124.6°).[27] As a result, the phenyl substituents are gently tilted from the subP plane with a dihedral angle of *ca.* 50.3°, while the phenyl dihedral angles are generally in the 70°−90° range in the case of TPP.[28]

The formation of H_2TPP was confirmed as a byproduct based on its characteristic color and absorption spectrum.[21] The molecular structure of the major byproduct with the intense absorption band at 510 nm in Figure 2 was confirmed by X-ray analysis to be a boron dipyrromethene complex with two methylphenyl moieties at the terminal α-positions.[29] The ORTEP drawing is shown in Figure 5c. The boron atom is tetrahedrally bound by a hydroxyl oxygen atom, an oxygen atom of the propionate group, and two pyrrole nitrogen atoms. The structure contains two terminal phenyl groups, which point in the same direction with propionate groups in between.

IR Spectroscopy. IR spectra were recorded in order to analyze the relationship between the observed spectra and the molecular structures. Some of the observed frequencies are described in the Experimental Section. Figure 6 displays the spectra of PhsubP (**2a**) and TLsubP (**2b**), together with that of ZnTPP. PhsubP (**2a**) and TLsubP (**2b**) are the most simple *meso*-triaryl subPs in structural terms so the fundamental frequencies inherent in the triarylsubporphyrin structure can be extracted more easily. Similar bands are observed at the following: 3445 (m), 2919−2921 (s), 2849−2851 (s), 1716−1732 (m), 1505−1515 (m), 1457−1458 (m), 1265−1267 (m), 1153 (s), 792 (m), and 727−729 (m) cm^{-1}, where "s" and "m" stand for strong and medium intensity, respectively. Of these, the band at 3445 cm^{-1} appears to arise from an axial OH, while the bands at *ca.* 2920 and 2850 cm^{-1} can be assigned to C−H stretching modes

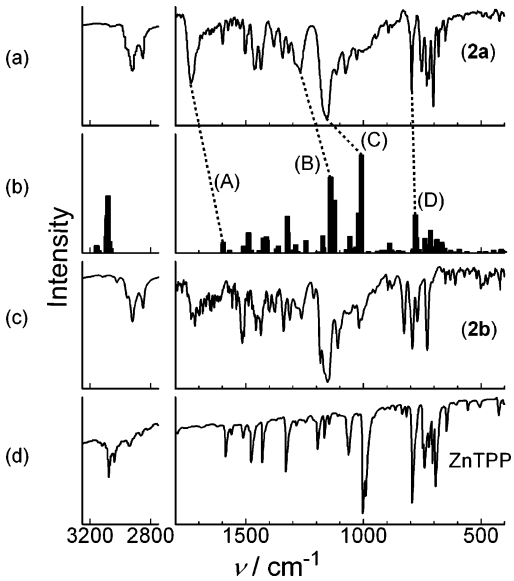

Figure 6. IR spectra of (a) PhsubP (**2a**), (b) calculated PhsubP (**2a**), (c) TLsubP (**2b**), and (d) ZnTPP.

of aromatic compounds (and of CH_3 in the case of TLsubP (**2b**)).[30] No band was observed between 2800 and 1750 cm^{-1}. The band at 1716−1732 (m) cm^{-1} is well resolved from the other bands and does not appear to correspond to any band in the ZnTPP spectrum. When this band is taken into consideration, the assignment of the other bands is not straightforward. In the case of TPPs,[31] many bands with medium intensity are observed in the 1100−1600, 950−1010, and 650−900 cm^{-1} regions. The bands in the 1100−1600 cm^{-1} region are assigned primarily to C═C, C−C, and C−N stretching and C−H bending modes. The bands in the 950−1010 cm^{-1} region are assigned to breathing modes of porphyrin and pyrrole, and deformation modes of the porphyrin skeleton, while the bands in the 650−900 cm^{-1} region are believed to arise from out-of-plane deformations of porphyrin and phenyl groups and in-plane deformations of porphyrin.[30] The IR spectra of PhsubP (**2a**) and TLsubP (**2b**) contain relatively similar patterns in the 600−900 cm^{-1} region.

Figure 6b contains the calculated IR spectrum of PhsubP (**2a**). The predicted vibrations above 2500 cm^{-1} have higher frequencies than those observed by experiment, as was observed during previous attempts[32] to use *ab inito* modeling to calculate porphyrin IR spectra. In the mid- and low-frequency region, however, both the relative and absolute frequency errors diminish and closer agreement with the calculation is obtained in terms of the overall intensity patterns. We attempted the vibrational assignment based on a comparison of simulated and experimental spectral peaks, rather than on individual peaks, since many normal modes are included. The 1716−1732 (m) band is assigned to C═C stretching modes of the phenyl groups.

(27) Scheidt, W. R.; Kasatner, M. E.; Hatano, K. *Inorg. Chem.* **1978**, *17*, 706.
(28) (a) Hoard, H. L. In *Porphyrins and Metalloporphyrins*; Smith, K. M., Ed.; Elsevier: Amsterdam, 1975, Chapter 8, pp 317−380 and many references therein. (b) Senge, M. O. In *The Porphyrin Handbook*; Kadish, K. M., Smith, K. M., Guilard, R., Eds.; Academic Press: San Diego, 2000; Vol. 10.
(29) Boron−dipyrromethene complex: $C_{32}H_{29}N_2B_1O_3$, M_W = 500.38, monoclinic, space group $P2_1/c$ (no. 14), a = 10.057(3) Å, b = 28.505(9) Å, c = 9.464(2) Å, β = 108.676(5)°, V = 2570.2(12) Å^3, Z = 4, ρ_{calcd} = 1.293 g/cm^3, T = −100 °C. R = 0.0733, R_w = 0.1604 (all data), GOF = 1.194.
(30) (a) Nakamoto, K. *Infrared Spectra of Inorganic and Coordination Compounds*; Wiley: New York, 1970. (b) Pouchert, C. J. *The Aldrich Library of Infrared Spectra*; Aldrich Co. Inc.: Milwaukee, WI, 1975.
(31) (a) Bour, P.; Zaruba, K.; Urvanova, M.; Sentnicka, V.; Matejka, P.; Fiedler, Z.; Kral, V.; Volka, K. *Chirality* **2000**, *12*, 191−198. (b) Li, X.-Y.; Czernuszewicz, R. S.; Kincaid, J. R.; Su, Y. O.; Spiro, T. G. *J. Phys. Chem.* **1990**, *94*, 31 and many references therein. (c) Li, W.; Wang, Y.-B.; Pavel, I.; Ye, Y.; Chen, Z.-P.; Luo, M.-D.; Hu, J.-M.; Kiefer, W. *J. Phys. Chem. A* **2004**, *108*, 6052. (d) Alben, J. O. In *The Porphyrins*; Dolphin, D., Ed.; Academic Press: New York; 1978; Vol. III, Chapter 7, pp 323−345.
(32) Tam, C. N.; Bour, P.; Keiderling, T. A. *J. Am. Chem. Soc.* **1996**, *118*, 10285.

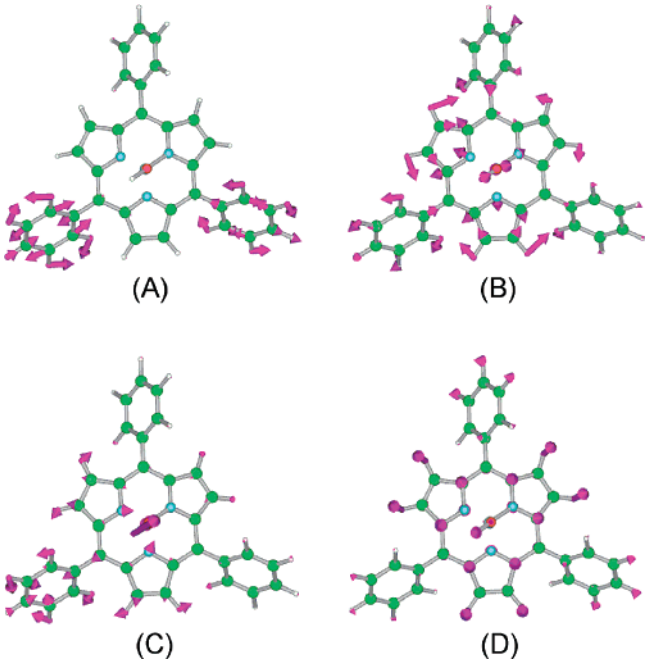

Figure 7. Some vibrational patterns calculated for PhsubP (**2a**) at (A) 1595, (B) 1138, (C) 1007, and (D) 778 cm^{-1}. These probably correspond to bands observed experimentally at 1733, 1267, 1153, and 793 cm^{-1}, respectively. In (D), most of the arrows are pointing upward.

This is over 100 cm^{-1} higher than the frequency of the corresponding band in TPP spectra. This may be related to the smaller rotation angle of the phenyl group from the subP plane. The 1265−1267 (m), 1153 (s), and 793 (s) bands are well-resolved and can be readily identified in both the simulated and experimental spectra. These are assigned, based on the simulation, as primarily arising from C−H bending of subP (+pyrrole deformation and symmetric), phenyl and pyrrole symmetric, and subP out-of-plane deformation vibrational modes, respectively, Figure 7. With respect to the fingerprint region, the following tentative assignments are made based on the calculation: *ca.* 1100−1600 cm^{-1}, C═C−C stretching of aryl and subP; *ca.* 830−1100 cm^{-1}, aryl C−H in-plane bending; *ca.* 660−790 cm^{-1}, aryl C−H in-plane bending plus subP core C−H in-plane bending; *ca.* 410−420 cm^{-1}, aryl and subP C═C−C out-of-plane bending or deformation vibration. In addition to these, the strong 1247 and 1174 cm^{-1} bands of MOsubP (**2e**) and 1072−1323 cm^{-1} bands of TFsubP (**2f**) that are not observed in other subPs could plausibly also be assigned to C−O−C asymmetric and symmetric stretching modes of the OMe group and to a C−F stretching mode of the CF_3 group, respectively, based on IR data reported previously.[30]

Electrochemistry. The CV and DPV curves of TLsubP (**2b**) and MOsubP (**2e**) are shown in Figure 8, together with the first oxidation and reduction potentials of five subPs derived from the DPV experiments. We could not detect first oxidation potentials for 4PysubP (**2c**), while only the CV and DPV of MOsubP (**2e**) contained the second reduction potentials. The first reduction occurred at *ca.* −2.1 to −1.8 V vs Fc^+/Fc, while the first oxidation potentials were detected at 0.45−0.85 V. Since the central boron atom does not participate in the redox process within the potential range used in this experiment,[33] the observed redox couples are ascribed to the subP ligand. Both oxidation and reduction couples shift depending on whether the *meso*-substituents are electron donating or withdrawing. For

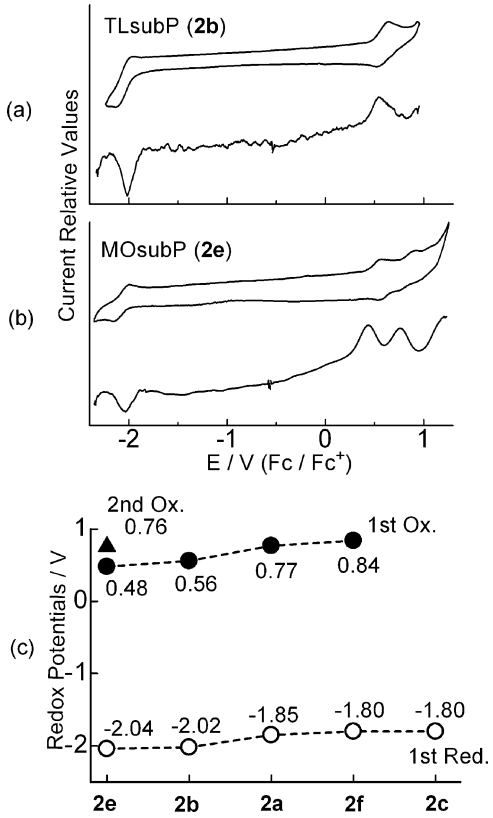

Figure 8. CV and DPV curves for (a) TLsubP (**2b**) and (b) MOsubP (**2e**) in *o*-DCB solutions containing 0.1 M TBAP as electrolyte. Scan speed = 100 and 10 mV/s for CV and DPV, respectively. (c) Redox potentials obtained from DPV experiments on subPs. The numbers indicate the potentials.

example, the redox couples of compounds having electron withdrawing groups appear at more positive potentials. The potential difference between the first oxidation and reduction is in the 2.52−2.64 V range (or 2.58 ± 0.06 V), which is larger than those observed for *meso*-tetraarylporphyrins (*ca.* 2.25 ± 0.05 V),[34] reflecting the ring contraction effect. This is consistent with the appearance of the UV−visible absorption bands at shorter wavelengths than those for the standard tetrapyrrole porphyrins. Comparison of the redox potentials with those of ZnTPP (first oxid = 0.30 and first redn = −1.75 V vs Fc^+/Fc)[35] suggests that the HOMOs of the subPs are more stable, while the LUMOs are destabilized.

Electronic Absorption and MCD Spectroscopy. The electronic absorption and MCD spectra of all six monomeric subPs and $(3PysubP)_2O$ (**3**) are displayed in Figure 9, while Figure 10 provides greater detail for the absorption spectra in the Q band region. The data are summarized in Table 1. The strong absorption in the 370−380 nm region is clearly similar to the Soret band of TPP and therefore almost certainly arises from a transition directly analogous to the B transition within Gouterman's four-orbital model. This band appears at a shorter wavelength in the case of compounds with electron withdrawing

(33) (a) del Rey, B.; Keller, U.; Torres, T.; Rojo, G.; Agullo-Lopez, F.; Nonell, S.; Marti, C.; Blasselet, S.; Ledoux, I.; Zyss. J. *J. Am. Chem. Soc.* **1998**, *120*, 12808. (b) Potz, R.; Goldner, M.; Huckstadt, H.; Cornelissen, U.; Tutass, A.; Hombgorg, H. *Z. Anorg. Allg. Chem.* **2000**, *626*, 588.
(34) (a) Kadish, K. M. *Rec. Prog. Inorg. Chem.* **1986**, *34*, 435. (b) Kadish, K. M.; Royal, G.; Gueletti, L. In *The Porphyrin Handbook*; Kadish, K. M., Smith, K. M., Guilard, R., Eds.; Academic Press: San Diego, 2000; Vol. 9, Chapter 59, pp 1−219.
(35) Rao, T. A.; Maiya, B. G. *Polyhedron* **1994**, *13*, 1863.

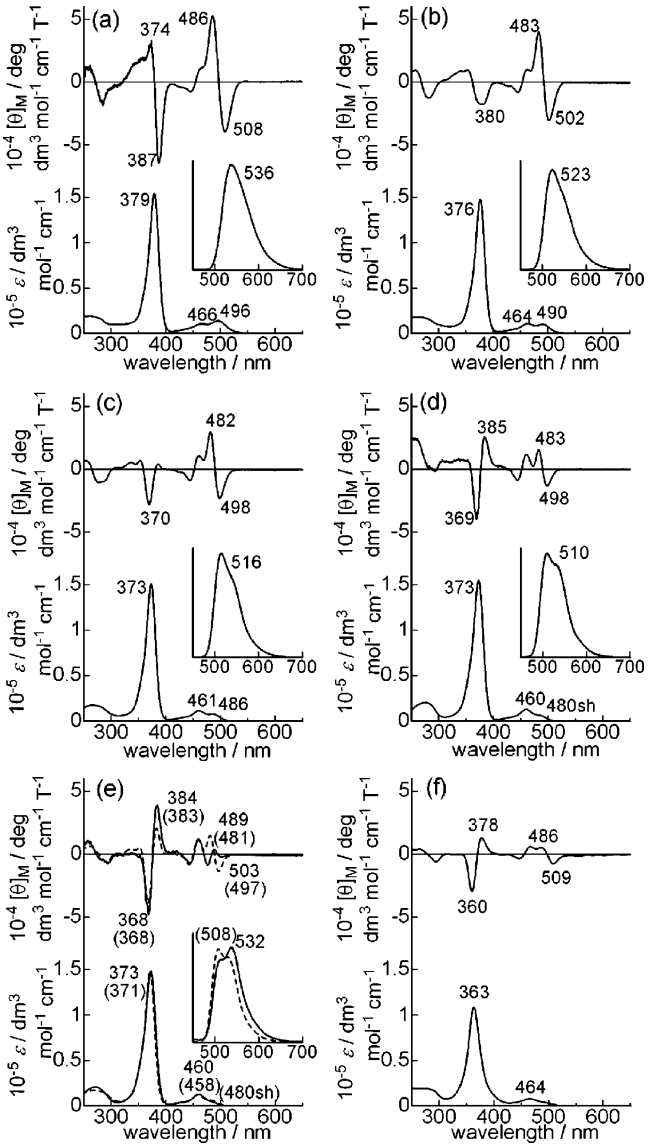

Figure 9. Electronic absorption, MCD, and fluorescence spectra of (a) MOsubP (**2e**), (b) TLsubP (**2b**), (c) PhsubP (**2a**), (d) TFsubP (**2f**), (e) 3PysubP (**2d**) (broken lines) and 4PysubP (**2c**) (solid lines), and (f) $(3PysubP)_2O$ (**3**) in $CHCl_3$ (absorption and MCD) and in EtOH (fluorescence).

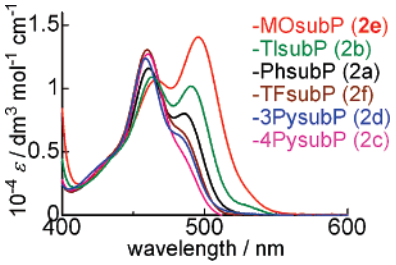

Figure 10. Electronic absorption spectra in the Q band region of MOsubP (**2e**), TLsubP (**2b**), PhsubP (**2a**), TFsubP (**2f**), 3PysubP (**2d**), and 4PysubP (**2c**) in $CHCl_3$.

substituents. The weaker absorption band in the 400−540 nm region can be assigned by direct inspection as almost certainly arising from a transition directly analogous to the Q transition within Gouterman's four-orbital model, since it is about an order of magnitude less intense. The Soret and Q bands, therefore, lie at considerably shorter wavelengths (*ca.* 30−50 and 70−100 nm, respectively) than the corresponding bands in the spectra of metallotetraphenylporphyrins (*ca.* 410−420 and 500−610 nm).[36] The absorption coefficient of the Soret band is *ca.* 25% that of ZnTPP in the same solvent.[37] The absorption spectra of the six subPs are generally similar in shape, with the exception of the Q_{00} band where there is greater intensity for compounds with electron donating *meso*-substituents (Figure 10). The weak Q_{00} intensity is related to the fact that the first and second HOMOs and LUMOs are degenerate or near degenerate. In the context of tetrapyrrole porphyrins, Gouterman's four-orbital model predicts that this results in a π-system, which mimicks that of a D_{16h} symmetry cyclic polyene, by having an allowed B and a forbidden Q band based on orbital angular momentum changes of $\Delta M_L = \pm 1$ and $\pm$ 9, respectively.[36,38] It is known that the Q_{00} bands of TPPs are generally weaker than those of octaethylporphyrins where there is greater separation of the first and second HOMOs. As a result, in TPPs, generally the Q_{00} band is weaker than the Q_{01} vibrational band, while, in OEPs, the Q_{00} and Q_{01} band have comparable intensities.

As shown in Figure 9f, the Soret absorption peak of the μ-oxo dimer is blue-shifted from that of the constituent monomer by 10 nm, while the Q-band peaks are slightly red-shifted, due to interaction between the Soret and Q excited states. The blue shift of the Soret band can be explained by exciton theory.[39]

In contrast with the electronic absorption spectra, the MCD spectra differ markedly from compound to compound. Although the absorption coefficient ratio of the Soret band to Q band in the absorption spectra is about 10:1, the relative Q band intensities in the MCD spectra are much larger, thus reflecting the greater orbital angular momentum associated with the excited state[40] of a forbidden $\Delta M_L = \pm 7$ transition (by analogy with Gouterman's four-orbital model for standard tetrapyrrole porphyrins).[38] The MCD spectra of the Q band region can be divided into two distinct groups. The subPs with electron donating groups show an intense −ve/+ve pattern in ascending energy (i.e. positive Faraday *A* term), while those with electron withdrawing groups are more complex with a concomitant decrease in intensity. The Soret band region MCD spectra can be divided into groups on a similar basis. The spectra of subPs with electron donating groups such as 4-methoxy and tolyl groups contain a −ve/+ve pattern as in the Q band region, while in contrast the spectra of subPs with electron withdrawing groups such as pyridyl and 4-(trifluoromethyl)phenyl contain a +ve/−ve pattern (i.e., a negative Faraday *A* term).[41] In addition, careful inspection reveals that the −ve/+ve Soret MCD pattern observed for MOsubP (**2e**) changes gradually on going to

(36) Gouterman, M. In *The Porphyrins*; Dolphin, D., Ed.; Academic Press: New York; 1978; Vol. III, Chapter 1, pp 1−165.
(37) Kobayashi, N.; Takeuchi, Y.; Matsuda, A. *Angew. Chem., Int. Ed.* **2007**, *46*, 758.
(38) (a) Gouterman, M. *J. Chem. Phys.* **1959**, *30*, 1139. (b) Gouterman, M. *J. Mol. Spectrosc.* **1961**, *6*, 138.
(39) Kasha, M.; Rawls, H. R.; El-Bayoumi, M. A. *Pure Appl. Chem.* **1965**, *11*, 371.
(40) (a) Piepho, S. B.; Schatz, P. N. *Group Theory in Spectroscopy with Applications to Magnetic Circular Spectroscopy*; Wiley: New York, 1983. (b) Stephens, P. J. *J. Chem. Phys.* **1970**, *52*, 3489. (c) Stillman, M. J.; Nyokong, T. In *Phthalocyanines-Properties and Applications*; Leznoff, C. C., Lever, A. B. P., Eds.; VCH: Weinheim, 1989, Chapter 3, pp 133−289.
(41) (a) Michl, J. *J. Am. Chem. Soc.* **1978**, *100*, 6801. (b) Ishii, K.; Kobayashi, N.; Matsuo, T.; Tanaka, M.; Sekiguchi, A. *J. Am. Chem. Soc.* **2001**, *123*, 5356.

Table 1. Absorption and MCD Data in $CHCl_3$

compound	absorption[a]	MCD[b]
PhsubP (**2a**)	486 (8000), 461 (12 000), 373 (151 000)	498 (−23 000), 482 (30 000), 461 (11 000), 444 (−8800), 386 (4100), 370 (−28 000)
TLsubP (**2b**)	490 (10 000), 463 (11 000), 376 (148 000)	502 (−30 000), 483 (40 000), 463 (10 000), 444 (−7900), 380 (−18 000), 353 (9600)
MOsubP (**2e**)	496 (14 000), 466 (11 000), 379 (154 000)	508 (−39 000), 486 (53 000), 466 (11 000), 446 (−7600), 387 (−64 000), 374 (33 000)
TFsubP (**2f**)	480 (7000), 460 (13 000), 373 (155 000)	498 (−13 000), 483 (15 000), 460 (12 000), 444 (−8700) 385 (25 000), 369 (−40 000)
4PysubP (**2c**)	460 (13 000), 373 (148 000)	503 (−2200), 489 (3800), 477 (−8600), 459 (12 000), 445 (−7000), 384 (39 000), 368 (−48 000)
3PysubP (**2d**)	480 (6400), 458 (12 000), 371 (149 000)	497 (−13 000), 481 (15 000), 459 (12 000), 443 (−8100), 383 (21 000), 368 (−38 000)
$(3PysubP)_2O$ (**3**)	464 (7700), 363 (109 000)	509 (−7500), 486 (5300), 467 (5900), 446 (−3300), 378 (13 000), 360 (−29 000)

[a] λ/nm (ϵ/dm^3 mol^{-1} cm^{-1}). [b] λ/nm ($[\theta]_M$/deg dm^3 mol^{-1} cm^{-1} T^{-1}).

Table 2. Fluorescence Data in Benzene and Ethanol

compound	λ_{MAX}/ 10^3 cm^{-1}	λ_{FLU}/ 10^3 [a] cm^{-1}	Φ_F in EtOH	Φ_F in benzene	$\Delta\nu$/ 10^3 [a] cm^{-1}
ZnTPP	16.9	16.7	-	0.03	0.20
PhsubP (**2a**)	20.6	19.4	0.07	0.12	1.21
TLsubP (**2b**)	20.4	19.1	0.07	0.11	1.27
MOsubP (**2e**)	20.2	18.7	0.07	0.11	1.51
TFsubP (**2f**)	20.8	19.6	0.06	0.10	1.23
4PysubP (**2c**)	-	18.8	0.06	0.11	-
3PysubP (**2d**)	20.8	19.7	0.06	0.10	1.15

[a] Ethanol solution.

TLsubP (**2b**) and then to PhsubP (**2a**). That is to say, the relative intensity of the positive envelope at higher energy becomes weaker, so that, in PhsubP, only the negative trough is observed. On going further to 3PysubP (**2d**), a positive MCD envelope develops at lower energy, and this intensifies in the case of TFsubP (**2f**), to the point in the case of 4PysubP (**2c**) that the positive and negative MCD envelopes have almost equal intensities. These drastic changes in MCD patterns depending on substituents are highly unusual. In the cases of subPcs[10c] and subAP,[25] only positive *A* terms were observed for the Q_{00} and Soret bands. Although, as described above, the MCD signal in the Soret band region of the PhsubP spectrum is not a typical Faraday *A* term, the presence of first-derivative-shaped Q_{00} and Soret bands of the other compounds strongly suggests that the excited states are still orbitaly degenerate,[40] as would be anticipated based on the effective C_3 symmetry of the subPs.

The MCD spectrum of the μ-oxo dimer does not differ significantly from that of the constituent monomers. In the case of $(3PysubP)_2O$ (**3**), the positive Faraday *A* term becomes more pronounced in the Q band region. The negative Faraday *A* term in the Soret band region is very similar to that of 3PysubP (**2d**).

Emission Spectroscopy. All six subPs reported in this study exhibit green fluorescence in the 480−670 nm region, upon excitation at any wavelength between 260 and 480 nm, with the main peak observed in the 508−536 nm region, Figure 9. As would be anticipated, the vibrational bands are more intense in the case of subP compounds, such as 4PysubP, which have strong Q_{01} absorption bands. The excitation spectra are all similar to the corresponding absorption spectra, Figure S4. The quantum yields (ϕ_F) of the S1 emission were determined to be 0.10−0.12 in benzene and 0.06−0.07 in ethanol, Table 2, due to the change in polarity. 9,10-Diphenyl anthracene was used as the calibrant ($\phi_F = 0.84$ in benzene).[13] These values are much larger than that of ZnTPP in benzene ($\phi_F = 0.03$).[42] The Stokes shifts for subPs were in the 1200−1500 cm^{-1} range as opposed to the *ca.* 200 cm^{-1} shift observed for ZnTPP. TriarylsubPs probably have more flexible structures.

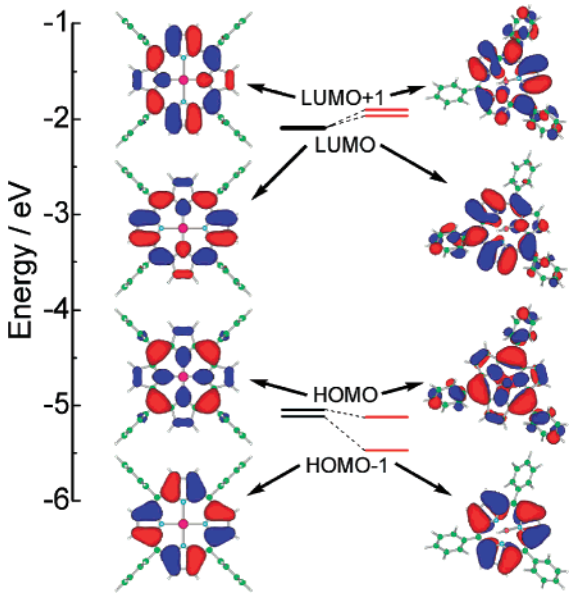

Figure 11. Calculated frontier MOs and MO energies of ZnTPP and PhsubP (**2a**). Note that there is almost no electron density on the phenyl group of ZnTPP, while the LUMOs and HOMO of PhsubP (**2a**) are fully delocalized to the phenyl group.

Molecular Orbital Calculations. MO calculations were performed for substituent-free subP, MOsubP (**2e**), PhsubP (**2a**), and 4PysubP (**2c**). The results were compared to those derived for ZnTPP calculated under the same conditions. Figure 11 provides a comparison of the frontier MOs and energy levels of ZnTPP and PhsubP (**2a**). The second HOMO (a_{1u}), first HOMO (a_{2u}), and LUMO (e_{gx}, e_{gy}) of the D_{4h} symmetry ZnTPP complex transform under the C_{3v} symmetry of PhsubP (**2a**) as a_1, a_2, and e, respectively. Since the inner ligand perimeter of subP contains a 12-atom 14-π-electron system, the $n = 3$ condition is satisfied in terms of the $4n + 2$ aromaticity rule. Three sets of alternating nodes are observed for the first HOMO and second HOMO, while four sets of alternating nodes are observed for the LUMOs of PhsubP (**2a**). This explicitly demonstrates that subPs can indeed be viewed as ring-contracted

(42) Seybold, P. G.; Gouterman, M. *J. Mol. Spectrosc.* **1969**, *31*, 1.

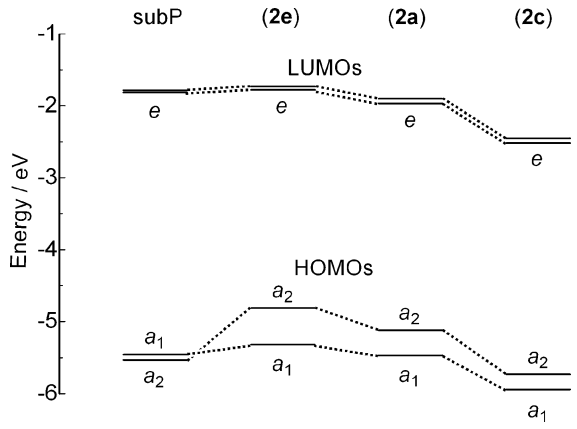

Figure 12. Energies calculated for the frontier π-MO levels of unsubstituted subP, MOsubP (**2e**), PhsubP (**2a**), and 4PysubP (**2c**). The second LUMO−first LUMO energy gap is always less than 0.07 eV, while the first HOMO−second HOMO energy gap values are 0.075, 0.506, 0.348, and 0.211 eV, respectively.

porphyrins and can be analyzed based on Gouterman's four-orbital model, since four and five sets of alternating nodes are observed for the corresponding MOs of metal porphyrin complexes based on the orbital angular momentum properties of the 16-atom 18-π-electron inner ligand perimeter. As would be anticipated based on the redox data, the LUMOs of PhsubP (**2a**) are destabilized while the first HOMO and second HOMO are stabilized relative to the four frontier π-MOs of ZnTPP. As can be demonstrated from the size of the MO coefficients, the HOMO and LUMOs of PhsubP (**2a**) are delocalized over the phenyl moiety, while the corresponding coefficients are almost zero in the case of the phenyl moieties of ZnTPP. There is clearly a much larger interaction between the central subP or porphyrin π-system and the phenyl moieties in the case of the subP systems. Several reasons can be inferred for this phenomenon. (i) In the case of TPPs, the angles reported between the phenyl group and porphyrin plane have consistently been greater than 70°[28] due to the steric hindrance between the hydrogen atoms at the ortho positions of the phenyl groups and those at the β-pyrrole positions. This effect was reproduced in the optimized structures in our DFT calculations with the rotational barrier calculated to be *ca.* 150 kcal mol^{-1} per phenyl group. In contrast, the corresponding angle was predicted to be in the 45°−55° range in the case of the triphenylsubporphyrins, since the steric hindrance is reduced. The distances between hydrogens at the *ortho*-positions of the phenyl groups and the β-pyrrole protons are significantly longer in the case of subPs, and the calculated rotational barrier is, therefore, reduced to *ca.* 20 kcal mol^{-1} per phenyl group. If this prediction is accurate, the $\pi-\pi$ interactions between the $2p_z$ carbon atomic orbitals of the *meso*-phenyl groups and the main subP π-system must become larger. (ii) The subP ligand is substantially smaller than the porphyrin tetrapyrole structure so the HOMO−LUMO energy gap of the phenyl groups is expected to be closer to that of subP (3.156 eV) than to that of tetraphenylporphyrin (2.951 eV).

In Figure 12, the energy levels of the frontier π-MOs of four of the subPs are compared. Since the B−O−H (OH = axial ligand) angle is not 180°, the first LUMO and second LUMO have slightly different energies. The energy gap is 0.048−0.065 eV. The MO energies are stabilized on going from the electron rich MOsubP (**2e**) compound to PhsubP (**2a**), and still further to the electron deficient 4PysubP (**2c**), since the electronic repulsion between the subP π-system and the aryl groups decreases in this order. In particular, the extent of stabilization of the first HOMO is more marked than that of the second HOMO, since there are large coefficients at *meso*-positions, thereby making the first HOMO−second HOMO energy gap smaller for subPs with electron withdrawing aryl groups. It should be noted that there is no coefficient at the *meso* position of the second HOMO. This is the reason that the Q_{00} bands of (trifluoromethyl)phenyl- and the pyridylsubporphyrins are weak. The first HOMO−second HOMO energy gap of MOsubP (**2e**), PhsubP (**2a**), and 4PysubP (**2c**) are calculated to be 0.51, 0.35, and 0.21 eV, respectively. Comparison of the substituent-free subP and PhsubP (**2a**) data suggests that the a_2 MO is destabilized by *meso*-phenyl substitution. This has been reported previously in the case of tetrapyrole porphyrins and TPPs.[36,38]

The coefficients of the one-electron transitions contributing to the Q and Soret bands are summarized in Table 3. From the magnitudes, it can clearly be seen that transitions between the four frontier π-MOs are the major contributing factor, as is the

Table 3. Calculated Transition Energies, Oscillator Strength (***f***), and Configurations of SubPs

compound	λ/nm[a]	*f*	wavefunction[b,c]	assignment
ZnTPP	525.4	0.0013	$0.517\|H \rightarrow L> - 0.491\|2^{nd}H \rightarrow 2^{nd}L> + ...$	Q
	525.4	0.0013	$0.517\|H \rightarrow 2^{nd}L> - 0.491\|2^{nd}H \rightarrow L> + ...$	Q
	369.9	1.2965	$0.301\|2^{nd}H \rightarrow L> + 0.280\|2^{nd}H \rightarrow 2^{nd}L> + 0.296\|H \rightarrow 2^{nd}L> - 0.250\|H \rightarrow L> + ...$	Soret
	369.9	1.2965	$0.301\|2^{nd}H \rightarrow 2^{nd}L> + 0.280\|2^{nd}H \rightarrow L> + 0.296\|H \rightarrow L> - 0.250\|H \rightarrow 2^{nd}L> + ...$	Soret
MOsubP (**2e**)	471.9	0.1707	$0.600\|H \rightarrow L> + 0.336\|2^{nd}H \rightarrow 2^{nd}L> + ...$	Q
	467.3	0.1382	$0.589\|H \rightarrow 2^{nd}L> - 0.360\|2^{nd}H \rightarrow L> + ...$	Q
	361.6	0.8272	$0.419\|2^{nd}H \rightarrow L> - 0.291\|2^{nd}H \rightarrow 2^{nd}L> + ...$	Soret
	358.6	0.8139	$0.436\|2^{nd}H \rightarrow 2^{nd}L> + 0.285\|2^{nd}H \rightarrow L> + ...$	Soret
PhsubP (**2a**)	458.1	0.0989	$0.576\|H \rightarrow L> - 0.386\|2^{nd}H \rightarrow 2^{nd}L> + ...$	Q
	453.5	0.0622	$0.557\|H \rightarrow 2^{nd}L> + 0.418\|2^{nd}H \rightarrow L> + ...$	Q
	352.5	0.8320	$0.481\|2^{nd}H \rightarrow L> - 0.317\|H \rightarrow 2^{nd}L> + ...$	Soret
	351.7	0.8120	$0.508\|2^{nd}H \rightarrow 2^{nd}L> + 0.281\|H \rightarrow L> + ...$	Soret
4PysubP (**2c**)	455.0	0.0637	$0.553\|H \rightarrow L> - 0.423\|2^{nd}H \rightarrow 2^{nd}L> + ...$	Q
	451.6	0.0315	$0.527\|H \rightarrow 2^{nd}L> + 0.458\|2^{nd}H \rightarrow L> + ...$	Q
	355.8	0.7811	$0.438\|2^{nd}H \rightarrow L> - 0.353\|H \rightarrow 2^{nd}L> + ...$	Soret
	355.1	0.7695	$0.473\|2^{nd}H \rightarrow 2^{nd}L> + 0.315\|H \rightarrow L> + ...$	Soret

[a] Excited states associated with spectral bands above 350 nm are shown. [b]Only the coefficients that are greater than 0.25 are shown. [c]H and L indicate HOMO and LUMO, respectively.

case with ZnTPP.[36,38] Strictly speaking, there is no configuration interaction (CI) in DFT calculations. However, since it is generally accepted[43] that there is little difference in the results of DFT and Hartree−Fock calculations, we can discuss the relative intensities of the Q_{00} bands conceptually using the coefficients in this table. The first HOMO → first LUMO and second HOMO → second LUMO transitions interact by CI to give the Q and Soret bands.[36,38] The Q band intensity is proportional to $|C_1\langle\text{HOMO}|e\mathbf{r}|\text{LUMO}\rangle - C_2\langle\text{second HOMO}|e\mathbf{r}|\text{second LUMO}\rangle|^2$ and $|C_3\langle\text{HOMO}|e\mathbf{r}|\text{second LUMO}\rangle - C_4\langle\text{second HOMO}|e\mathbf{r}|\text{LUMO}\rangle|^2$. When the separation of the first and second HOMOs is small, there is a close agreement in the energies of the transitions expressed by this equation, so that C_1 (or C_3) and C_2 (or C_4) values approach each other resulting in a reduction in the Q_{00} band intensity. The C_1 (or C_3) values in Table 3 become smaller, while C_2 (or C_4) values become larger on going from MOsubP (**2e**) to PhsubP (**2a**), and then to 4PysubP (**2c**). As a result, the difference between C_1 (or C_3) and C_2 (or C_4) is smallest for 4PysubP (**2c**), which is consistent with the experimentally observed Q_{00} band of this compound being the least intense. The oscillator strength, ***f***, of the calculated Q bands in Table 3 also decreases in this order. The wavelength values are also consistent with the experimental observation that both the Q and Soret bands appear at longer wavelengths in the presence of electron donating *meso*-substituents.

Conclusion

We have reported the synthesis of *meso*-triarylsubPs. The synthesis was based on adding tripyrrolylborane to refluxing propionic acid containing arylaldehyde. A rigorous and tedious purification procedure based on multiple chromatography steps was required to obtain the triarylsubporphyrins in *ca.* 4−8% yield. The main byproduct was confirmed by X-ray crystallography to be a boron dipyrromethene with two methylphenyl moieties at the terminal α-positions. All six subPs show Soret and Q band-like absorption bands in the 370−380 and 400−540 nm regions, respectively, and these bands have been interpreted on the basis of MO calculations within the conceptual framework of Gouterman's four-orbital model.[36] The MCD spectra are characteristic of porphyrin congeners, but the Soret band region MCD spectra are markedly different from those of tetrapyrrole porphyrins, since the Faraday *A* terms change their sign from −ve/+ve for subPs with electron donating aryl groups to +ve/−ve for subPs with electron withdrawing *meso*-aryl groups. SubPs in this study exhibit green fluorescence in the 490−620 nm region, and their quantum yields were 0.10−0.12 in benzene and 0.06−0.07 in ethanol, which are larger than that for ZnTPP (0.03 in benzene)[42] and comparable to that of metal-free tetraphenylporphyrin (0.11 in benzene).[42] IR spectra were assigned on the basis of DFT calculations. The bands observed at 1267 and 797 cm^{-1} were assigned primarily to C−H bending and out-of-plane deformation vibrational bands arising from the subP skeleton. The difference in potential between the first oxidation and reduction steps is *ca.* 2.6 V, which is larger than those of conventional porphyrins (2.25 ± 0.05 V), reflecting the smaller π-conjugated system. A μ-oxo subP was also synthesized and characterized.

Acknowledgment. N.K. expresses deep gratitude to Prof. W. S. Durfee, Buffalo State Collage, for discussions on the synthetic method of subporphyrins and to Dr. S. Shimizu for the collection of X-ray data of TFsubP (**2f**). This research was partially supported by a Grant-in-Aid (17350063) for Scientific Research and the COE project, Giant Molecules and Complex Systems, 2006, from the Ministry of Education, Science, Sports and Culture, Japan. Some of the calculations were performed using supercomputing resources at the Information Synergy Center, Tohoku University.

Supporting Information Available: Electronic absorption and fluorescence spectra of the boron dipyrrromethene byproduct, experimental and calculated mass spectra for the subPs, HMBC spectra of TLsubP (**2b**) and MOsubP (**2e**), and fluorescence and excitation spectra of subPs in this study. A complete version of ref 15 is also provided. This material is available free of charge via the Internet at http://pubs.acs.org.

JA0712120

(43) Mack, J.; Asano, Y.; Kobayashi, N.; Stillman, M. J. *J. Am. Chem. Soc.* **2005**, *127*, 17697. Mack, J.; Stillman, M. J.; Kobayashi, N. *Coord. Chem. Rev.* **2007**, *251*, 429.